Research Article | Vol. 25, No. 6 | 20 Mar 2017 | OPTICS EXPRESS 6664

Optics EXPRESS

Liquid-cooled Ti:Sapphire thin disk amplifiers for high average power 100-TW systems

R. S. NAGYMIHALY,[1,*] H. CAO,[1] D. PAPP,[1] G. HAJAS,[1] M. KALASHNIKOV,[1,2] K. OSVAY,[1] AND V. CHVYKOV[1]

[1]*ELI-HU Non-Profit Ltd., Dugonics tér 13, H-6720 Szeged, Hungary*
[2]*Max Born Institute for Nonlinear Optics and Short Pulse Spectroscopy, Max-Born-Strasse 2a, 12489 Berlin, Germany*
[*]*Roland.Nagymihaly@eli-alps.hu*

Abstract: In this work, numerical heat transfer simulations of direct water-cooled gain modules for thin disk (TD) Ti:Sapphire (Ti:Sa) power amplifiers are presented. By using the TD technique in combination with the extraction during pumping (EDP) method 100-TW class amplifiers operating around 300 W average power could be reached in the future. Single and double-sided cooling arrangements were investigated for several coolant flow velocities. Simulations which upscale the gain module for multiple kilowatts of average power were also performed for large aperture Ti:Sa disks and for multiple disks with several coolant channels.

OCIS codes: (140.7090) Ultrafast lasers; (140.3280) Laser amplifiers; (140.6810) Thermal effects.

References and links

1. V. V. Lozhkarev, G. I. Freidman, V. N. Ginzburg, E. V. Katin, E. A. Khazanov, A. V. Kirsanov, G. A. Luchinin, A. N. Malshakov, M. A. Martyanov, O. V. Palashov, A. K. Poteomkin, A. M. Sergeev, A. A. Shaykin, and I. V. Yakovlev, "Compact 0.56 Petawatt laser system based on optical parametric chirped pulse amplification in KD*P crystals," Laser Phys. Lett. **4**(6), 421–427 (2007).
2. E. W. Gaul, M. Martinez, J. Blakeney, A. Jochmann, M. Ringuette, D. Hammond, T. Borger, R. Escamilla, S. Douglas, W. Henderson, G. Dyer, A. Erlandson, R. Cross, J. Caird, C. Ebbers, and T. Ditmire, "Demonstration of a 1.1 petawatt laser based on a hybrid optical parametric chirped pulse amplification/mixed Nd:glass amplifier," Appl. Opt. **49**(9), 1676–1681 (2010).
3. J. H. Sung, S. K. Lee, T. J. Yu, T. M. Jeong, and J. Lee, "0.1 Hz 1.0 PW Ti:sapphire laser," Opt. Lett. **35**(18), 3021–3023 (2010).
4. T. J. Yu, S. K. Lee, J. H. Sung, J. W. Yoon, T. M. Jeong, and J. Lee, "Generation of high-contrast, 30 fs, 1.5 PW laser pulses from chirped-pulse amplification Ti:sapphire laser," Opt. Express **20**(10), 10807–10815 (2012).
5. Y. Chu, X. Liang, L. Yu, Y. Xu, L. Xu, L. Ma, X. Lu, Y. Liu, Y. Leng, R. Li, and Z. Xu, "High-contrast 2.0 Petawatt Ti:sapphire laser system," Opt. Express **21**(24), 29231–29239 (2013).
6. J. H. Sung, S. K. Lee, H. W. Lee, J. Y. Yoo, and C. H. Nam, "Development of 0.1 Hz 4.0 PW Laser at CoReLS," in *Conference on Lasers and Electro-Optics*, OSA Technical Digest (2016) (Optical Society of America, 2016), paper SM1M.3.
7. Y. Arikawa, S. Kojima, A. Morace, S. Sakata, T. Gawa, Y. Taguchi, Y. Abe, Z. Zhang, X. Vaisseau, S. H. Lee, K. Matsuo, S. Tosaki, M. Hata, K. Kawabata, Y. Kawakami, M. Ishida, K. Tsuji, S. Matsuo, N. Morio, T. Kawasaki, S. Tokita, Y. Nakata, T. Jitsuno, N. Miyanaga, J. Kawanaka, H. Nagatomo, A. Yogo, M. Nakai, H. Nishimura, H. Shiraga, S. Fujioka, H. Azechi, A. Sunahara, T. Johzaki, T. Ozaki, H. Sakagami, A. Sagisaka, K. Ogura, A. S. Pirozhkov, M. Nishikino, K. Kondo, S. Inoue, K. Teramoto, M. Hashida, and S. Sakabe, "Ultrahigh-contrast kilojoule-class petawatt LFEX laser using a plasma mirror," Appl. Opt. **55**(25), 6850–6857 (2016).
8. W. P. Leemans, J. Daniels, A. Deshmukh, A. J. Gonsalves, A. Magana, H. S. Mao, D. E. Mittelberger, K. Nakamura, J. R. Riley, D. Syversrud, C. Toth, and N. Ybarrolaza, "Bella laser and operations," in *Proceedings of PAC2013* (2013), paper THYAA1.
9. K. Yamakawa, M. Aoyama, S. Matsuoka, T. Kase, Y. Akahane, and H. Takuma, "100-TW sub-20-fs Ti:sapphire laser system operating at a 10-Hz repetition rate," Opt. Lett. **23**(18), 1468–1470 (1998).
10. Y. H. Peng, Y. X. Lim, J. Cheng, Y. Guo, Y. Y. Cheah, and K. S. Lai, "Near fundamental mode 1.1 kW Yb:YAG thin-disk laser," Opt. Lett. **38**(10), 1709–1711 (2013).
11. C. J. Saraceno, F. Emaury, C. Schriber, M. Hoffmann, M. Golling, T. Südmeyer, and U. Keller, "Ultrafast thin-disk laser with 80 μJ pulse energy and 242 W of average power," Opt. Lett. **39**(1), 9–12 (2014).
12. H. Fattahi, H. G. Barros, M. Gorjan, T. Nubbemeyer, B. Alsaif, C. Y. Teisset, M. Schultze, S. Prinz, M. Haefner, M. Ueffing, A. Alismail, L. Vámos, A. Schwarz, O. Pronin, J. Brons, X. T. Geng, G. Arisholm, M. Ciappina, V. S. Yakovlev, D.-E. Kim, A. M. Azzeer, N. Karpowicz, D. Sutter, Zs. Major, T. Metzger, and F. Krausz, "Third-generation femtosecond technology," Optica **1**(1), 45–63 (2014).

#282889 https://doi.org/10.1364/OE.25.006664
Journal © 2017 Received 14 Dec 2016; revised 27 Jan 2017; accepted 27 Jan 2017; published 14 Mar 2017

Optics EXPRESS

13. P. F. Moulton, "Spectroscopic and laser caracteristics of Ti:Al_2O_3," J. Opt. Soc. Am. B **3**(1), 125–133 (1986).
14. E. R. Dobrovinskaya, L. A. Lytvynov, and V. Pishchik, *Sapphire: Material, Manufacturing, Applications* (Springer, 2009).
15. S. Chénais, F. Druon, S. Forget, F. Balembois, and P. Georges, "On thermal effects in solid-state lasers: The case of ytterbium-doped materials," Prog. Quantum Electron. **30**(4), 89–153 (2006).
16. V. Chvykov, R. S. Nagymihaly, H. Cao, M. Kalashnikov, and K. Osvay, "Design of a thin disk amplifier with extraction during pumping for high peak and average power Ti:Sa systems (EDP-TD)," Opt. Express **24**(4), 3721–3733 (2016).
17. V. Chvykov and K. Krushelnick, "Large aperture multi-pass amplifiers for high peak power lasers," Opt. Commun. **285**(8), 2134–2136 (2012).
18. V. Chvykov, H. Cao, R. Nagymihaly, M. P. Kalashnikov, N. Khodakovskiy, R. Glassock, L. Ehrentraut, M. Schnuerer, and K. Osvay, "High peak and average power Ti:sapphire thin disk amplifier with extraction during pumping," Opt. Lett. **41**(13), 3017–3020 (2016).
19. www.eli-alps.hu
20. www.comsol.com
21. F. R. Menter, "Two-equation eddy-viscosity turbulence models for engineering applications," AIAA J. **32**(8), 1598–1605 (1994).
22. F. R. Menter, M. Kuntz, and R. Langtry, "Ten years of industrial experience with the SST turbulence model," in *Turbulence Heat and Mass Transfer 4* (2003).
23. R. B. Bird, W. E. Stewart, and E. N. Lightfoot, *Transport Phenomena* (John Wiley & Sons, 2007).
24. T. L. Bergman, A. S. Lavine, F. P. Incropera, and D. P. Dewitt, *Fundamentals of Heat and Mass Transfer* (John Wiley & Sons, 2011).
25. P. Ferrara, M. Ciofini, L. Esposito, J. Hostaša, L. Labate, A. Lapucci, A. Pirri, G. Toci, M. Vannini, and L. A. Gizzi, "3-D numerical simulation of Yb:YAG active slabs with longitudinal doping gradient for thermal load effects assessment," Opt. Express **22**(5), 5375–5386 (2014).
26. J. Tapping and M. L. Reilly, "Index of refraction of sapphire between 24 and 1060 °C for wavelengths of 633 and 799 nm," J. Opt. Soc. Am. A **3**(5), 610–616 (1986).
27. G. M. Hale and M. R. Querry, "Optical constants of water in the 200-nm to 200-μm wavelength region," Appl. Opt. **12**(3), 555–563 (1973).
28. Z. Ye, C. Liu, B. Tu, K. Wang, Q. Gao, C. Tang, and Z. Cai, "Kilowatt-level direct-'refractive index matching liquid'-cooled Nd:YLF thin disk laser resonator," Opt. Express **24**(2), 1758–1772 (2016).

1. Introduction

Present day state-of-the-art ultrafast laser systems, using table-top arrangements, have reached the several PW peak power [1–7]. The majority of these systems rely on amplification using Ti:Sapphire (Ti:Sa), a gain crystal, which has exceptional spectral and thermal properties [3–6]. Ti:Sa, unlike amplification based on nonlinear optical crystals, can be efficiently pumped by second harmonic pulses of Nd:YAG or Nd:YLF lasers, which can produce high pulse energy at a high repetition rate. An important feature of Ti:Sa amplification is that the gain medium is not sensitive to the temporal shape and the temporal jitter of the pump pulses, and pump pulse duration can be much larger than the length of the seed pulses (up to hundreds of nanoseconds), unlike optical parametric amplification (OPA). Unfortunately, Ti:Sa amplification has a significant drawback – heating in the crystal can cause thermal lensing and even fractures within the medium because of the non-uniform transverse temperature profile when cooling the side face of the crystal. This limitation prevents Ti:Sa lasers from high repetition rate operation. Petawatt lasers typically run in single shot mode or up to 1 Hz [3–6,8], whilst 100-TW class lasers can reach 10 Hz repetition rate [9]. This relatively low operation frequency gives rise to a rather long data-acquisition time in the case of several experiments and prevents these systems from numerous industrial and medicinal applications.

Thin disk (TD) technology may offer the possibility for Ti:Sa crystals to be used in high average output power systems [10,11] because the longitudinal direction of heat extraction greatly reduces thermal lensing and also ensures scalability. Research and development has strongly focused on relatively narrow emission spectral band media (doped YAGs) and thus the pulse duration has been limited to the lower, sub-picosecond regime [12]. There are additional issues with these laser media including low longitudinal gain due to low thickness, active ion doping concentration and emission cross section, which lead to very complicated optical schemes with many passes for both pump and seed pulses. The application of TD technology to Ti:Sa increases the longitudinal gain and thus reduces the number of passes.

Optics EXPRESS

The combination of broadband pulse amplification and high repetition rate operation due to the much larger spectral bandwidth of 200 nm (FWHM) and thermal conductivity of 34.5 W/m/K at 300 °K would ultimately redefine the limits of conventional amplifier arrangements [13,14]. The thermal conductivity of Ti:Sa is much higher than generally used TD gain media, like Yb:YAG with its 11 W/m/K value at 300 °K [15], so the thickness of the crystal can be larger for the same thermal conditions. In this configuration, the suppression of the transverse amplified spontaneous emission (TASE) and the transverse parasitic generation (TPG) are the primary challenges.

In our previous work [16] a combination of the TD amplifiers with the Extraction During Pumping method [17] (EDP) was suggested. This would maintain the broad bandwidth and minimize energy losses associated with TPG and TASE in thin crystals whilst overcoming the thermal effects associated with the high repetition rate. Numerical simulations related to the EDP-TD Ti:Sa amplifiers were performed for different geometries and amplification parameters. Experimental testing of an EDP-TD amplifier based on Ti:Sa was recently performed [18]. The final cryogenically cooled Ti:Sa amplifier in a 100 TW/10 Hz/28 fs laser system was replaced with a room temperature cooled EDP-TD Ti:Sa arrangement. Amplified seed pulse energy of 2.6 J was reached with only three passes using 0.5 J of input and 5 J of absorbed pump energy. Temperature measurements in the Ti:Sa crystal showed that the heat extraction capability of this scheme supports much higher repetition rates and as well as pulse energies.

In this paper, the heat transfer in a 100 TW-level 100 Hz Ti:Sa EDP-TD amplifier with reflective and transmissive optical schemes is simulated in detail and the upscaling to even higher average power is considered. The results will contribute to the development of the high energy, high repetition rate laser channel of the Extreme Light Infrastructure - Attosecond Light Pulse Source (ELI-ALPS) facility [19].

2. Model

This work focuses on room temperature water-cooled amplifier heads in order to keep the operation of the system as simple as possible and to increase the mechanical stability, as no vacuum technology is used. Cost of a water-based cooling system is also below that of the gas-based or cryogenic solutions. However, high flow velocities by the cooled surface are required for sufficient heat extraction from the gain crystal. The finite element method (FEM) from COMSOL Multiphysics software [20] was used to calculate the heat extraction in the amplifier head in a two part model. The heating by the pump pulses and heat extraction by the coolant was simulated with the Heat Transfer (HT) part with the computation of the coolant flow development was coupled to the HT part. The experimentally obtained parameters in [18] were used to validate our model. We used an approximation of the coolant channel from the experiment and simulated the heat extraction in case of pumping with 4 J energy pulses at 10 Hz repetition rate without amplification. The simulation showed good agreement with the experimentally measured temperature values under similar conditions.

2.1. Geometry

A single channel cooling concept with reflective optical scheme [Fig. 1(a)] and a double channel cooling concept with a transmissive optical scheme [Fig. 1(b)] were investigated. In case of the single-channel concept, the front surface was assumed to have an antireflection (AR) coating for both seed and pump wavelengths. The rear surface of the Ti:Sa crystal has a high reflection (HR) layer resulting in the reflection of the pump and seed beams from the rear surface. This works as an active mirror with the rear side of the gain crystal in direct contact with the coolant flow [Fig. 1(a)] for heat extraction. Simulations were also performed for double channel cooled arrangements where both optical surfaces of the crystal were AR-coated for the same wavelength combination as in case of the single channel concept [Fig.

Optics EXPRESS

1(b)]. Both optical surfaces of the crystal were in direct contact with the coolant as the seed and pump beams pass through the coolant.

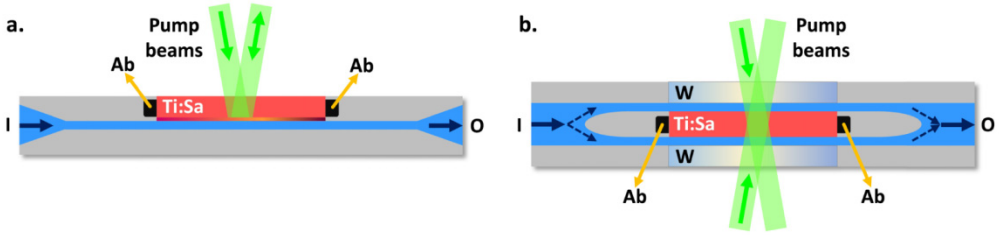

Fig. 1. Schematic picture of the two types of cooling arrangements. Single channel cooling with reflection based optical scheme (a), when the rear optical surface of the Ti:Sa disk is HR coated. Double channel cooling with a transmission based optical scheme (b), where the front and rear surfaces of the Ti:Sa disk are AR coated. I is the inlet and O is outlet for coolant, while W is window and Ab is absorber material to reduce Fresnel reflection. The material visualized with grey is metal, and with blue is the coolant.

In this case, both seed and pump beams have to propagate through the coolant two times per pass, which means, these beams are exposed to beam distortions caused by the flow disturbances. However, if one can design the flow to be smooth enough, these disturbances can be mitigated to a low level.

2.2. Laser parameters

The focus of this paper is the development of the final amplifier of a 100-TW class laser system at the ELI-ALPS facility. The amplifier is envisioned to generate output energy of 3 J when pumped by 6 J laser pulses at 100 Hz repetition rate. At this performance level, the average power of the output seed and the heating power of the pump laser are both around 300 W. Based on safety considerations and our experimental experience [18], both seed and pump beam diameters were taken to be 19.5 mm in the crystal, which corresponds to a maximal total pump fluence of 2 J/cm^2 for both the reflection and transmission schemes. To account for the maximal heating effect in the gain medium, 50% of the pump energy is assumed to be dissipated as heat during the amplification process. The mitigation of transverse lasing was accounted for by applying the EDP technique with 3 passes of the seed pulses (effectively 6) in case of the reflection scheme, while in case of the transmission scheme, a 4 pass arrangement was considered as the thickness of the Ti:Sa disk had increased. The coatings on the disk for both reflective and transmissive cases were taken into account in our models.

2.3. Flow simulation

The maximal thermal load is concentrated in the center of the disk during the amplification process. For this reason, the 2D analysis consisted of the central cross section of the amplifier crystal and the coolant channel in the amplifier head. A Shear Stress Transport (SST) model [21,22] was used to simulate the flow inside the channel as a high precision in the heat transfer between the crystal and the coolant is required. This model does not use wall functions in areas close to the walls, which means the flow profile in the boundary layer is not assumed but calculated from the governing equations. The size of the complete geometry is around 60 cm × 6.5 cm × 6 cm, which would require vast amount time to solve the SST model equations, especially with high accuracy and heat transfer coupling. For this reason, the standard k-ω model for the complete channel with moderate precision is initially solved to generate the flow profile. The geometry was then reduced to the center section of the channel where the coolant is in contact with the gain medium. Virtual boundaries were created at the cut lines of the complete channel, from which the one closer to the channel inlet was dedicated as the inlet boundary of the central part model. By coupling the output of the k-ω to the SST model, the development of the flow was resolved in a short distance after the inlet

Optics EXPRESS

boundary. This technique resulted in a higher precision and faster convergence of the flow computation than the case of defining a uniform velocity distribution with a mean velocity value at the inlet boundary.

The scope of this work is to identify the limits of direct water cooling combined with the TD geometry so here we only give the base equations for the SST turbulent model, on which our final calculations were based. The transport equations for k (turbulent kinetic energy) and ω (specific dissipation rate) can be written as

$$\frac{\partial(\rho k)}{\partial t}+\frac{\partial(\rho U_i k)}{\partial x_i}=\tilde{P}_k-\rho\beta^* k\omega+\frac{\partial}{\partial x_i}\left[(\mu+\sigma_k\mu_T)\frac{\partial k}{\partial x_i}\right], \quad (1)$$

$$\frac{\partial(\rho\omega)}{\partial t}+\frac{\partial(\rho U_i\omega)}{\partial x_i}=\alpha\rho S^2-\rho\beta\omega^2+\frac{\partial}{\partial x_i}\left[(\mu+\sigma_\omega\mu_T)\frac{\partial\omega}{\partial x_i}\right]+2(1-F_1)\frac{\rho\sigma_{\omega 2}}{\omega}\frac{\partial k}{\partial x_i}\frac{\partial\omega}{\partial x_i}, \quad (2)$$

where ρ is the density, μ is the viscosity of the fluid and U_i denotes the velocity field components [21]. A production limiter, which prevents the build-up of turbulence in stagnation regions, is defined as

$$P_k=\mu_T\frac{\partial U_i}{\partial x_j}\left(\frac{\partial U_i}{\partial x_j}+\frac{\partial U_j}{\partial x_i}\right)\rightarrow\tilde{P}_k=\min\left(P_k,10\cdot\beta^* k\rho\omega\right). \quad (3)$$

F_1 is a blending function, which is equal to zero far from the walls, and tends to one inside the boundary layer. These behaviors are inherited from the k-ε and k-ω models, respectively. The turbulent eddy viscosity is defined by

$$\mu_T=\frac{a_1 k}{\max\left(a_1\omega, S\,F_2\right)}, \quad (4)$$

Where $\boldsymbol{S}$ is the invariant measure of the strain rate and F_2 is a second blending function. All constants present in the model are calculated by using a blending function from the corresponding constants of the k-ε and k-ω models via

$$\alpha=\alpha_1 F+\alpha_2(1-F). \quad (5)$$

The constants used in these calculations are $\beta^*=0.09$, $a_1=0.31$, $\alpha_1=5/9$, $\beta_1=3/40$, $\sigma_{k1}=0.85$, $\sigma_{\omega 1}=0.5$, $\alpha_2=0.44$, $\beta_2=0.0828$, $\sigma_{k2}=1$, $\sigma_{\omega 2}=0.856$ [22].

Equations (1) and (2) were solved for the stationary case and the compressibility of the fluid was neglected. The coolant fluid was chosen to be water. At the inlet of the channel, a normal (perpendicular to the input cross section of the channel) inlet velocity distribution and a temperature boundary condition, to account for keeping the inlet coolant temperature at a constant value of 15 °C, were applied. At the outlet, a pressure boundary condition was used with zero pressure. The walls in the complete geometry were taken to be thermally insulated except for the contact boundary between the crystal and the fluid. The size of the coolant channel was shaped to obtain a smooth velocity profile in front of the crystal, in order to get optimal heat extraction. Where possible, symmetry boundary conditions were used to ease the computational requirements. The cooling conditions for different inlet flow velocities were investigated to obtain the necessary heat extraction efficiency. The necessary mesh density was reached by checking the built-in boundary variable of dimensionless distance to cell center [20] in every model.

All material properties of both the Ti:Sa and water are considered to be temperature dependent and coupled fluid flow-heat transfer simulations were necessary as the viscosity of

Optics EXPRESS

the water has strong temperature dependency. The temperature-dependent material properties used in the simulations were from the COMSOL Material Library [20].

2.4. Heat transfer simulation

The calculation of the heat transfer was coupled to the flow simulation, where the heat equation for solid and fluid heat transfer was solved. The stationary heat transfer equation in fluids is

$$\rho C_p \mathbf{u} \cdot \nabla T + \nabla \cdot \mathbf{q} = Q + Q_p + Q_{vd}, \tag{8}$$

with

$$\mathbf{q} = -k \nabla T, \tag{9}$$

where $\mathbf{u}$ is the velocity vector, ρ is the fluid density, C_p is the specific heat capacity at constant pressure, T is the absolute temperature, $\mathbf{q}$ is the heat flux by conduction, and k is the thermal conductivity [23,24]. The terms on the left hand side are the heat advection and conduction terms, respectively. The terms at the right hand side of Eq. (8) are: Q is the heat source term

$$Q_p = \alpha_p T \cdot \mathbf{u} \cdot \nabla p \tag{10}$$

is the work done by pressure changes, and

$$Q_{vd} = \tau : \nabla \mathbf{u} \tag{11}$$

is the viscous dissipation term, where α_p is the thermal expansion coefficient, p is the pressure, and τ is the viscous stress tensor.

The stationary heat equation for solids can be written as

$$\nabla \cdot \mathbf{q}_s = Q_s, \tag{12}$$

where Q_s is the volumetric heat source term in the solid, which accounts for the heating from the pump beam. Similar to Eq. (9), $\boldsymbol{q}_s$ is defined by

$$\mathbf{q}_s = -k_s \nabla T_s, \tag{13}$$

where k_s is the thermal conductivity and T_s is the absolute temperature of the solid material. The heat source in this model was the absorbed pump power, where the pump beam was defined analytically like in [16], and its radial profile was taken to be super-Gaussian (20th order) with a constant radius along the complete crystal thickness. Absorption of the pump beam was based on the Beer-Lambert law and accounted for multiple passes through the crystal. Half of the absorbed pump power was assumed to be dissipated as heat, with the remainder amplifying the seed beam and extracted optically from the system, accounting for 50% amplification efficiency. Since the pump beams provided by state-of-the-art high energy pump lasers have flat-top transversal profile with high uniformity, we assumed a homogeneous pump depletion over the pumped area in the Ti:Sa crystal. The absorption level of the pump pulses was kept at 95% level by changing the number of passes for the pump beam through the crystal, while the absorption coefficient of the disk was chosen to be 2.5 cm^{-1} for both schemes. As stated in [16], it is important to reach a uniform distribution of absorbed pump energy along the longitudinal direction of the crystal i.e., the direction perpendicular to the front and rear optical surfaces.

Optics EXPRESS

3. Results for 100-TW class amplifiers

3.1. Single channel cooling – reflective scheme

Direct liquid cooling on one (reflective) optical surface of the crystal has the advantage that neither pump nor seed beams have to pass through the coolant. This means that no wavefront distortion is coming directly from the coolant disturbances. However, this cooling technique requires a reflection based optical scheme, which places a high optical quality (surface flatness and roughness) demand on the HR coated back surface of the amplifier crystal. To suppress the energy loss from TPG and TASE, an absorber material dissolved in a refractive index matching liquid (RIL) at the edge of the gain material was applied with combination of the EDP method. The chamber for this liquid has to be carefully designed in order for a complete cover on the edge of the crystal without compromising the smoothness of the coolant channel whilst being compatible with the RIL fluid chamber design. Based on our modeling [16] and in previous EDP-TD amplifier experiments [18], an amplifier head with a Ti:Sa crystal of 35 mm diameter and 3 mm thickness, was used. Two passes for the pump pulses was assumed which was effectively four passes because of the back reflections from the crystal.

The coolant channel in the complete gain module was simulated with using the *k-ω* model for optimization of the design. The complete coolant channel was visualized in Fig. 2. We found, that the optimal width of the central part of the coolant channel to be 2 mm, which was suitable for efficient heat extraction and as well as structural purposes. The first section of the channel (diffusor and confusor) was designed for a uniform flow profile before the central section. This enabled the detailed conjugate heat transfer model to only simulate the developing, contact and out coupling zone of the channel without losing precision. The results of the k-ω model were coupled to the inlet boundary of the central part model's coolant channel.

Fig. 2. 2D model of the coolant channel geometry with the Ti:Sa crystal. CPB1 and CPB2 are boundaries of the central part of the model.

The curved part in the channel after the developing zone was designed to keep the width of the channel constant – a flange for holding the crystal and sealing the RIL fluid chamber was needed. Inlet flow velocities of 0.17, 0.25, 0.33, 0.42 and 0.5 m/s were used as the input to the modeled geometry.

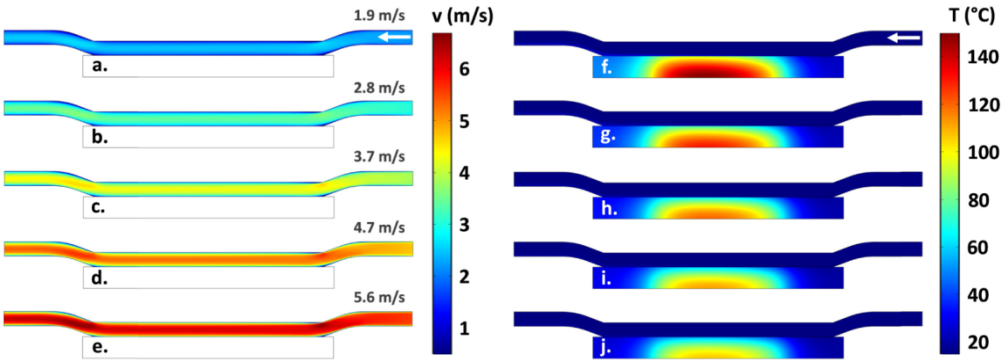

Fig. 3. Simulated velocity magnitude in the center section of the channel (gain crystal presented with only boundary lines) calculated with the SST model for different inlet velocities of the

Optics EXPRESS

complete channel (a-e). Inlet flow velocities of the center section were indicated at the input of the channels in case of (a-e). Temperature distributions obtained with the corresponding flow velocity in the crystal and the center section of the channel (f-j).

The velocity profiles presented in Fig. 3 demonstrates that a smooth and favorable velocity distribution in the contact region with the Ti:Sa disk [Figs. 3(a)-(e)]. Temperature distributions for the flow velocities were calculated in the central part of the complete geometry [Figs. 3(f)-(j)]. The temperature profile in the Ti:Sa disk is noticeably improved by increasing the flow velocity in the coolant channel. The coolant and initial temperature in the geometry was set to 15 °C. The temperature increase (TI), i.e. the difference between maximum temperature in the disk and the initial temperature of 15 °C, induced by pump energy dissipation also drops severely, which is presented in Fig. 4.

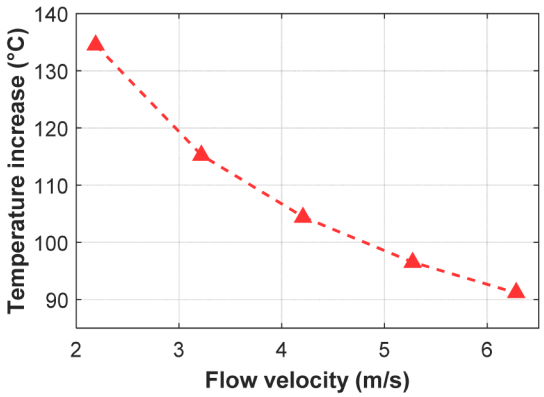

Fig. 4. TI within lasing crystal for different peak flow velocities in front of the Ti:Sa disk.

A temperature increase of 134.5 °C can be reached for a flow velocity of 2.2 m/s in the central part of the coolant channel. Raising the flow velocity to 6.3 m/s results in reducing the TI down to 91.2 °C.

The optical path difference (OPD) caused by the temperature change in the Ti:Sa crystal for a single pass was calculated for the 6.3 m/s flow velocity case (Fig. 5). Contributions of the thermal expansion and mechanical stress induced birefringence [25] were not included in this simplified OPD model. However, the distribution of temperature in the disk is smooth in the pumped region and these contributions should be much lower than in case of conventional rod type amplifiers.

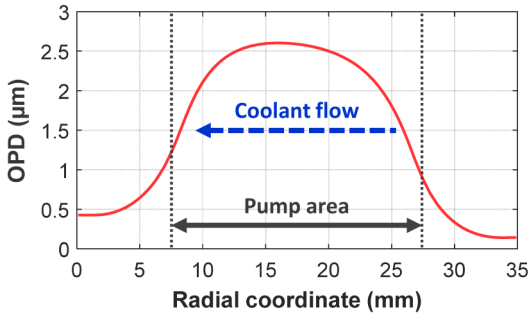

Fig. 5. Optical path difference caused by the thermal load in case of the single channel (one side) cooled 3 mm thick crystal. OPD was calculated in the central cross section parallel with the flow direction.

Changes in the refractive index of Ti:Sa caused by temperature increase were calculated at 799 nm wavelength and were based on [26]. The OPD profile is not symmetric, however this

Optics EXPRESS

beam distortion could be compensated by using a deformable mirror. The pumped area was marked in Fig. 5, which highlights the region of the crystal that will affect the wavefront of the seed pulses. As it can be seen in Fig. 5, the OPD curve is slightly tilted because the heat extraction capability of the water flow decreases gradually along the flow direction, which suggests larger amounts of coolant is needed to achieve ideal beam quality. There are two options, either increase the flow velocity, which may introduce turbulence, or increase the channel number, which will be discussed in the following.

3.2. Double channel cooling – transmissive scheme

More effective heat extraction can be accomplished by cooling both optical surfaces of the gain medium. Figure 6 shows our design of a double channel cooling system, tested with the same laser parameters as the single side cooling system.

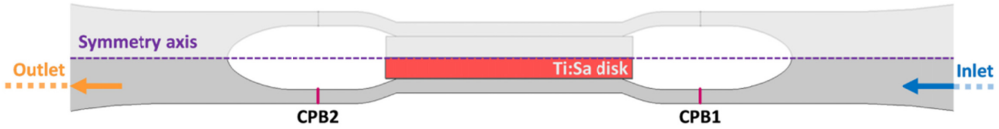

Fig. 6. 2D model of the double coolant channel geometry with a 6 x 35 mm Ti:Sa crystal. CPB1 and CPB2 are boundaries of the central part of the model.

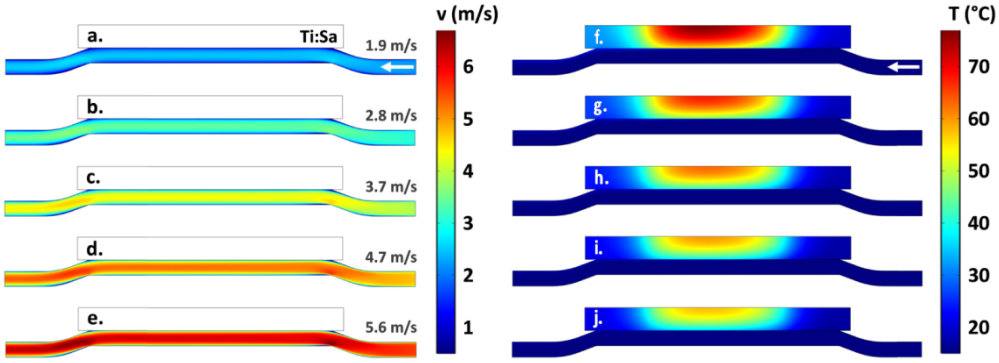

Fig. 7. Simulated velocity magnitude in the center section of half of the channel (gain crystal presented with only boundary lines) calculated with the SST model for different inlet velocities of the complete channel (a-e). Inlet flow velocities of the center section were indicated at the input of the channels in case of (a-e). Temperature distributions obtained with the corresponding flow velocities in half of the disk center section of the channel (f-j).

Computational time was saved by only modeling the coolant flow in half of the complete design and using symmetry boundary conditions at the symmetry axis of the geometry as shown in Fig. 6. The optical arrangement in the cooling scheme was changed the original reflection type to a transmission type scheme. Two thicknesses of the Ti:Sa crystal were investigated. 6 mm was initially chosen as it corresponds to the unfolded case of the single channel design. Pumping was performed by two passes from both sides in this case. A disk with 4 mm thickness was also simulated based on two considerations: suppression of parasitic lasing with the EDP technique can be still managed, and on the other hand, by decreasing the thickness, the cooling efficiency is improved further. With this thickness, the number of passes for the pump beam was increased to three with the assumption of two side pumping. For both 6 mm and 4 mm disk cases, the absorption level of 95% was reached for the pump pulses. Absorption of the pump and seed pulses in the coolant was neglected in our model, since its heating effect is negligible based on the low absorption coefficient of water [27].

Simulations were performed with the same flow velocities used in the single channel cooling simulations. However, the inlet velocities at the input of the geometry presented in

Optics EXPRESS

Fig. 6 are twice as fast as the single channel model due to the double channel contraction ratio being half of the single channel case. It is worth mentioning, that based on our simulation results, no turbulence was present in any part of the coolant channel. Velocity magnitude and temperature distributions in half of the central part of the simulated geometry are shown in Fig. 7.

The dual channel system makes an impressive change on the maximum measured TI. The TI values in case of different flow velocities for both the 6 and 4 mm thick disks are shown in Fig. 8. At 2.2 m/s flow velocity, the TI for the 6 mm disk reaches 61.5 °C, and by increasing the velocity to 6.3 m/s, the TI decreases to 42.5 °C.

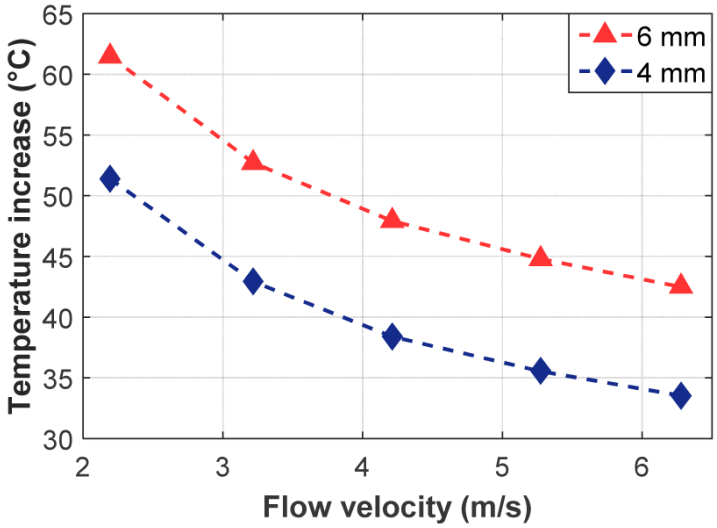

Fig. 8. Simulated temperature increase values for different peak flow velocities in front of the Ti:Sa disk. Results for disk size of 6 x 35 mm are plotted with red and for 4 x 35 mm disk size with blue.

Switching to the disk with 4 mm thickness results in serious improvement in thermal management performance. By using a flow velocity of 2.2 m/s in the contact zone, the peak temperature drops by 10.1 °C relative to the 6 mm disk and this relative improvement is maintained when flow velocity is increased to 6.3 m/s. Figure 7 shows, once more, that there is an asymmetric temperature distribution caused by the change of the heat extraction efficiency along the radial direction of the crystal. This effect can be explained with the thermal boundary layer development in the coolant along the crystal surface. However, this asymmetry decreases significantly at higher flow velocities, especially above 5.2 m/s.

OPD generated by the temperature profile through the temperature dependency of the refractive index was calculated for both 4 and 6 mm thick gain media in case of 6.3 m/s coolant flow velocity (Fig. 9). During the experimental work presented in [18], the wavefront distortion induced by the coolant flow for different channel thicknesses was measured and found negligible. Based on this knowledge, the effect of the coolant flow on the OPD was neglected in our model.

Optics EXPRESS

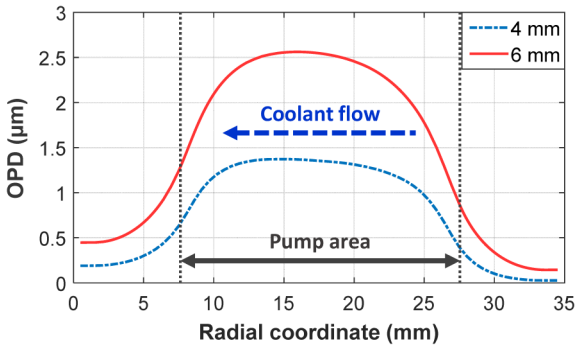

Fig. 9. Optical path difference caused by the thermal load in case of the 4 (blue), and 6 mm (red) thick crystals. The inlet flow velocity was taken to be 1 m/s for both cases.

Figure 9 shows that significant improvement can be achieved in the OPD profile in both the amplitude and flatness by using the disk with 4 mm thickness.

4. Results for scalability of direct liquid cooling

The results discussed in Section 3 focused on peak power, pump energy and repetition rate. The parameters of this system were chosen, according to our experimental experience, to demonstrate that a 10 Hz system could be upgraded to 100 Hz without sacrificing the beam quality. The next section looks at expanding experimental parameters in which TD could be deployed for systems with more pulse energy and thus higher average power. Temperature of the coolant was set to 15 °C for all the upscaling simulations. As a moderate inlet flow velocity, which practically equals to the peak value in the contact area of the channel, 4 m/s was set for all these simulations.

4.1. Increase of the disk diameter for higher energy

The pump energy, diameter and the crystal thickness all need to be increased in order for higher output energy. The optimal crystal diameter and thickness aspect ratio of 10 was found in our previous work for the sake of parasitic lasing suppression [16]. Temperature profiles were calculated for various repetition rates up to 100 Hz.

For a more comprehensive study, the scalability of the EDP-TD method with direct water cooling was explored.

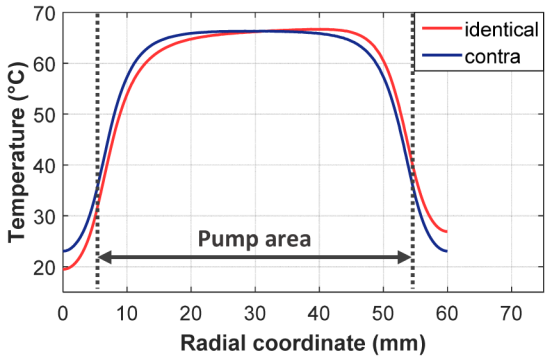

Fig. 10. Temperature profiles in the horizontal direction, in the center of the disks in case of the identical (red curve) and contra-directional (blue curve) flow cooling. The modeled amplifier contained a disk with a size of 6 x 60mm.

Increasing the diameter of the disk results in an increase in heating power which requires a greater pump energy in order to keep a constant total 2 J/cm^2 pump fluence. The modeled

Optics EXPRESS

geometry was simplified so that it only includes the crystal in direct contact with the 2 flat flow channels without any mounting. The same flow simulation technique is used as in Section 3. During the upscaling simulations, contra-directional flows were implemented in the two channels which resulted in more symmetric temperature profiles than a uniform flow direction in the two channels (Fig. 10). Changing the flow direction in one of the channels would be an engineering challenge but there would be significant improvements in the profile symmetry. The contra-directional flows were implemented in all upscaling simulations to show that it can improve the temperature profile.

Disks with diameters ranging from 6 to 20 cm and corresponding thicknesses of 0.6 cm to 2 cm, (corresponding to the aspect ratio of 10) were investigated where the safe operation limit could be defined by the level of wavefront distortion, which could be still compensated after the gain module (Fig. 11). The inlet flow velocity was 4 m/s in all cases to ensure high levels of heat extraction from the disk gain modules. Repetition rates of 20, 40, 60, 80 and 100 Hz were investigated for all disk sizes. Figure 11(a) shows that up to 40 Hz of operation every gain module would remain under 45 °C of TI relative to the coolant temperature. There is a significant rise in the TI when the repetition rate is increased further. However, the temperature profile would remain smooth and flat in the region of the laser amplification. By taking a compressor with an efficiency of 60% and compressed pulse duration of 20 fs, peak power of up to 8.5 PW and an average power of 17 kW could be reached [Fig. 11(b)].

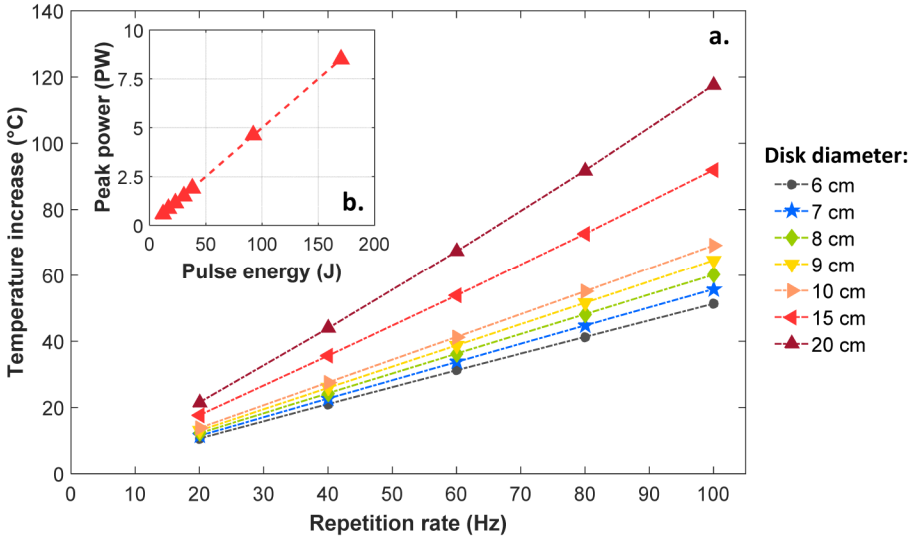

Fig. 11. Temperature increase in the disk for different repetition rates of operation and various disk sizes (a). Pump energy for the given diameters starting from 6 cm are the following: 40 J, 57 J, 77 J, 101 J, 127 J, 308 J, 567 J, respectively. Peak power of compressed pulses reached by amplification with the pump energies listed above (b), where 60% for compressor efficiency, 100 Hz for repetition rate and 20 fs for compressed pulse duration were taken into account.

4.2. Increase of the disk number for higher repetition rate

Further increases of the repetition rate could be achieved by splitting the gain disk to multiple plates with reduced thickness and increasing the number of coolant channels. For example using two crystals cooled on both optical surfaces results in double the number of cooled surfaces whilst the total absorbed pump power remains the same, thus evenly distributing the heating between two disks. If the thickness of the individual disks supports proper mounting and absorber chamber housing, the number of disks can be increased, which makes the further improvement of these systems quite straightforward [28].

Optics EXPRESS

Simulation results that demonstrate the capabilities of multiple disk EDP-TD amplifier modules are presented. Contra-directional flow arrangements were used in simulations for disks with 6, 10, 15 and 20 cm diameters. In all cases the thick disks are split into two plates of equal thickness and pumping beam diameters were also scaled up accordingly.

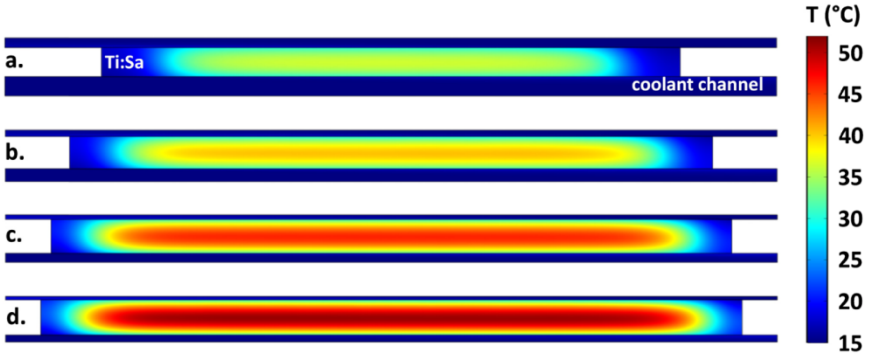

Fig. 12. Temperature distribution in half of the double disk amplifier module with 3 x 60 mm (a), 5 x 100 mm (b), 7.5 x 150 mm (c), 10 x 200 mm (d) Ti:Sa crystals. The disks are cooled by three channels.

Absorption coefficients were optimized in order to reach the previous absorption level of 95% in the total gain module with two passes for two-side pumping. Pump pulse energies are kept the same only in the case of increasing the diameter of the disk. The temperature profiles were simulated at 100 Hz repetition rate to show the potential of this method. Only half of the geometry was included in this model as a symmetry boundary condition was used in the center of the second coolant channel. Figure 12 shows that increasing the diameter and number of the disks results in a smoother distribution of the developed temperature. This is favorable for amplification to avoid any beam profile degradation. Comparing the TI development for different disk sizes shows that the double disk arrangements are more suitable to handle high average power pumping in power amplifiers (Fig. 13). In case of a 6 x 60 mm disk amplifier the TI reaches 51.3 °C and 21.5 °C for single and double disk modules, respectively and the difference between these two module types increases with disk size. This means that the heat extraction efficiency is increasing radically because of the larger cooled surface of the disks.

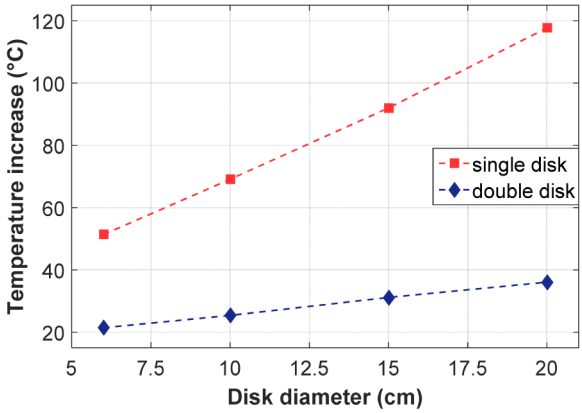

Fig. 13. Temperature increase in the single and double disk modules with Ti:Sa crystals of 6 cm, 10 cm, 15 cm and 20 cm diameters, cooled by three channels using 4 m/s flow velocity at the inlet boundary of the channels. The repetition rate is 100 Hz for all cases.

Optics EXPRESS

This is also observable for increases in the disk diameter. Figure 13 shows that there is a significant drop (81.6 °C) in the TI from the single disk scenario (117.7 °C) to the double disk arrangement (36.1 °C).

5. Conclusions and outlook

The results of numerical simulations on the thermal aspects of amplifier modules, which can be critical for 100-TW class thin disk Ti:Sa power amplifiers with an average power of around 300 W, have been presented. Our modeling showed that for 100 Hz operation, a TI of 91.2 °C relative to the coolant temperature of 15 °C can occur in case of a single coolant channel gain module. However, in a double coolant channel arrangement with optimized thickness of the disk this can be reduced to 33.5 °C with a flat temperature distribution along the radial coordinate of the disk. These results were obtained with 2D modeling of the coolant flow and heat transfer in the amplifier modules. Based on the 2D temperature maps in the central cross section of the disks, we expect slight astigmatism to be present in the seed beam after amplification, caused by the tilted temperature profile. This could be investigated with 3D simulations, which were beyond the scope of this work.

Simulations for larger peak power amplifier modules with double channel cooling were also conducted. Based on the TIs obtained, the maximal repetition rate at which the amplifiers could be operated safely without serious beam degradation can be estimated. By simply increasing the diameter, whilst maintaining the aspect ratio of the gain disks, extremely efficient heat extraction can be obtained with two coolant channels and thus flat temperature profiles with high repetition rate operation.

The thermal management of four gain modules with disk sizes ranging from 6 cm to 20 cm was investigated, when the single disk with two coolant channel scheme was changed for a double disk with three coolant channel arrangement. Based on these results, 2 kW output average power with a TI in the disks of 21.5 °C, while for an amplifier with an average power of 28 kW and a TI of 36 °C could be obtained in the future using multiple disks and cooling surfaces, also proper coolant flow conditions. Application of solid absorbers at the edge of the Ti:Sa disks could lead to much simpler mounting, which eventually would give rise to amplifier modules with several disks and simple channel formations.

Funding

The authors would like to acknowledge funding from ELI-ALPS with project number GINOP-2.3.6-15-2015-00001.

Acknowledgment

Portions of this work were presented at the Advanced Solid State Lasers Conference in 2016, in the paper titled “High Repetition Rate for Ultra-High Peak Power Laser Systems”.